JACS
JOURNAL OF THE AMERICAN CHEMICAL SOCIETY
Article
pubs.acs.org/JACS

In Vivo Fluorescence Imaging in the Second Near-Infrared Window with Long Circulating Carbon Nanotubes Capable of Ultrahigh Tumor Uptake

Joshua T. Robinson,[†] Guosong Hong,[†] Yongye Liang, Bo Zhang, Omar K. Yaghi, and Hongjie Dai*

Department of Chemistry, Stanford University, Stanford, California 94305, United States

Supporting Information

ABSTRACT: Cancer imaging requires selective high accumulation of contrast agents in the tumor region and correspondingly low uptake in healthy tissues. Here, by making use of a novel synthetic polymer to solubilize single-walled carbon nanotubes (SWNTs), we prepared a well-functionalized SWNT formulation with long blood circulation (half-life of ~30 h) in vivo to achieve ultrahigh accumulation of ~30% injected dose (ID)/g in 4T1 murine breast tumors in Balb/c mice. Functionalization dependent blood circulation and tumor uptake were investigated through comparisons with phospholipid-PEG solubilized SWNTs. For the first time, we performed video-rate imaging of tumors based on the intrinsic fluorescence of SWNTs in the second near-infrared (NIR-II, 1.1−1.4 μm) window. We carried out dynamic contrast imaging through principal component analysis (PCA) to immediately pinpoint the tumor within ~20 s after injection. Imaging over time revealed increasing tumor contrast up to 72 h after injection, allowing for its unambiguous identification. The 3D reconstruction of the SWNTs distribution based on their stable photoluminescence inside the tumor revealed a high degree of colocalization of SWNTs and blood vessels, suggesting enhanced permeability and retention (EPR) effect as the main cause of high passive tumor uptake of the nanotubes.

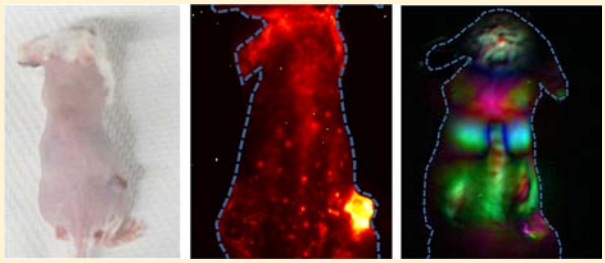

INTRODUCTION

The field of nanomedicine has grown rapidly in recent years.[1,2] Nanoparticles have been used to enhance traditional medicine in the area of disease detection, prevention, and treatment.[3−5] In vivo tumor imaging represents one of the areas where nanotechnology has shown promising results. Single-walled carbon nanotubes (SWNTs) exhibit intrinsic photoluminescence (PL) in the near-infrared (NIR) light region, known as the desirable "biological window" because of the low optical scattering,[6,7] absorption,[8] and autofluorescence[9,10] by endogenous tissues in this range.[9,11] The large Stokes shift of 400−500 nm for SWNTs also allows for imaging with low background.[12] In vivo fluorescent imaging has inherent advantages due to its quick feedback and high spatial resolution.[13] Dynamic contrast-enhanced fluorescence imaging may also facilitate tumor imaging and differentiation of tumor from surrounding normal tissues and organs.[11] It is known that tumors behave differently from normal tissues with fenestration of blood vessels[14,15] inside tumors. Vessel imaging could serve as the basis for distinguishing tumor area from normal tissues.

The unique optical properties of SWNTs make them useful in vivo fluorescent imaging agents. Proper functionalization with amphiphilic surfactant imparts SWNTs with high biocompatibility, affording stealth particles that avoid rapid removal by the body's immune system.[16,17] SWNTs have been used for drug delivery,[18] photoacoustic imaging,[19,20] NIR photoluminescence imaging,[21] and photothermal therapy.[17,22] Properly functionalized SWNTs can afford high tumor uptake through the enhanced permeability and retention (EPR) effect even without targeting agents.[23,24] Here, using relatively large 90 kDa amphiphilic poly(maleic anhydride-alt-1-octadecene)-methoxy poly(ethylene glycol) [C_{18}-PMH-mPEG][25] coating for nanotubes, we were able to achieve unprecedented 30% injected dose per gram of tumor accumulation of SWNTs. Although a significantly higher molecular weight C_{18}-PMH-mPEG has been previously used to coat SWNTs for long circulation time,[16,17,22] our current work has optimized the size of the starting C_{18}-PMH to achieve one of the highest nanoparticle tumor accumulation levels to date. The 90 kDa C18-PMH-mPEG coated the SWNT noncovalently, which preserved the intrinsic NIR photoluminescence and strong Raman graphitic "G" band of the SWNTs and allowed for in vivo imaging and ex vivo quantification of the pharmacokinetics. Other studies examined covalent functionalization of SWNTs. Oxidized SWNTs with carboxylic acids were linked to PEG, and 1,3-dipolar cycloaddition was also used for PEGylation of SWNTs.[26,27] Covalently functionalized SWNTs were promising for cancer therapeutics delivery[28] but diminished the intrinsic spectroscopic signatures of SWNTs for imaging and tracking.

We performed ex vivo imaging of tumor slices for 3D reconstruction of the tumor based on the intrinsic fluorescence of SWNTs in the second NIR region (1.1−1.4 μm), revealing

Received: April 24, 2012
Published: June 5, 2012

   dx.doi.org/10.1021/ja303737a | J. Am. Chem. Soc. 2012, 134, 10664−10669

the distribution of SWNTs inside the tumor and probing the degree of penetration of SWNTs inside the tumor. We also showed that high-frame-rate video imaging with dynamic contrast facilitated by principal component analysis (PCA) is a novel approach to distinguish tumor from normal tissues based on their different blood circulating behaviors. It has been reported that high-frame-rate video imaging based on the fluorescence of organic fluorophores and SWNTs can be combined with PCA to dynamically enhance the contrast of different normal organs and increase the anatomical resolution of mice.[11,29] Because of angiogenesis[30] during growth of a tumor, which contains many newly born, fenestrated vessels,[31] blood flows differently in tumor tissue than in normal tissue, making the tumor distinguishable from normal organs based on video imaging and PCA, as reported here for the first time.

RESULTS AND DISCUSSION

To make water-soluble and biocompatible SWNT suspension, we bath-sonicated HiPCO (Unidym) SWNTs in poly(maleic anhydride-*alt*-1-octadecene)-poly(ethylene glycol) methyl ether [C_{18}-PMH-mPEG], a 90 kDa[25] amphiphilic surfactant with about nine repeating units (Figure 1a, see Experimental Details for synthesis). Details of the preparation for individual, water-soluble SWNTs can be found in the Supporting Information. The UV−vis−NIR absorption spectrum (Figure 1b) of the resulting SWNT suspension has multiple peaks corresponding to van Hove singularity transitions of different chiralities, suggesting a stable, well-suspended solution of nanotubes. Figure 1c shows the photoluminescence versus excitation (PLE) spectrum of the SWNT suspension, where the four chiralities indicated by the arrows are the most likely ones to be excited by an 808 nm laser because of resonance. The photoluminescence quantum yield of the SWNTs used in this work was ~0.1%, as the tube suspension was made by direct sonication in surfactant solutions.[9] An up to ~30-fold increase in quantum yield could be obtained by a surfactant exchange method.[9] A Raman scattering spectrum of the SWNTs upon excitation of 785 nm exhibited strong graphitic band (G band) resonance,[26] which is characteristic of graphitic carbon materials including SWNTs (Figure 1d).

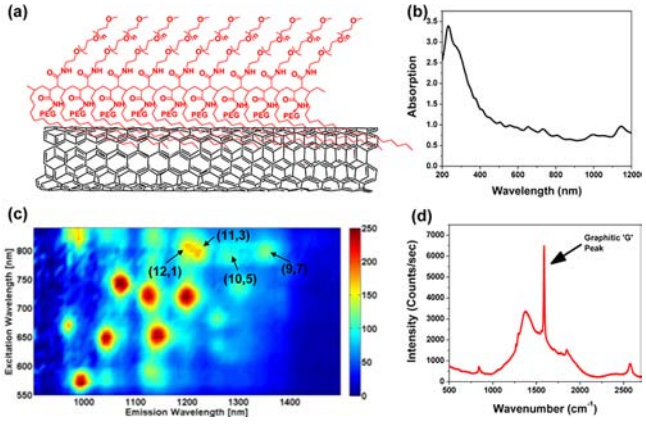

Figure 1. Characterization of C_{18}-PMH-mPEG (90 kDa) coated SWNTs: (a) schematic of the water-soluble SWNT conjugate; (b) UV−vis−NIR absorption spectrum of the suspension; (c) 2D photoluminescence versus excitation (PLE) map of a C_{18}-PMH-mPEG (90 kDa) coated SWNTs, with different chirality SWNTs showing up as bright spots; (d) Raman scattering spectrum of the SWNT suspension excited by a 785 nm laser. The graphitic band (G band) is indicated by an arrow at ~1600 cm^{-1}.

A 200 μL suspension of SWNT at ~0.35 mg/mL (~3.5 mg/kg dose) was injected intravenously into a mouse with a subcutaneous xenograft 4T1 murine tumor located on the right hind limb. Video-rate fluorescent images based on the intrinsic NIR-II fluorescence of SWNTs in the 1.1−1.4 μm region upon excitation of 808 nm were taken continuously right after injection to track SWNT blood circulation in real time up to 210 s postinjection (pi), as shown in the first Supporting Information video file. An exposure time of 100 ms enabled us to capture images at a frame rate of ~8 frame/s (including an overhead time of ~19 ms in readout). The first Supporting Information video file revealed the path of SWNTs through the body, showing blood circulating to the lungs and heart through the veins to be oxygenated (Figure 2a) before being pumped into other organs including kidneys and liver through arteries (Figure 2b). Interestingly, besides the normal organs that were lit up by SWNT fluorescence, SWNT fluorescence in the 4T1 tumor started to appear at 8.0 s pi and increased in intensity over time (Figure 2c). At 15.1 s pi, major vessels inside the tumor showed up (Figure 2d). Clearer vascular structure in the tumor area could be identified from 20 to 30 s pi (Figure 2e). After 60 s pi, the tumor region could be distinguished from nearby normal tissues because of the clear outline of the tumor (Figure 2f).

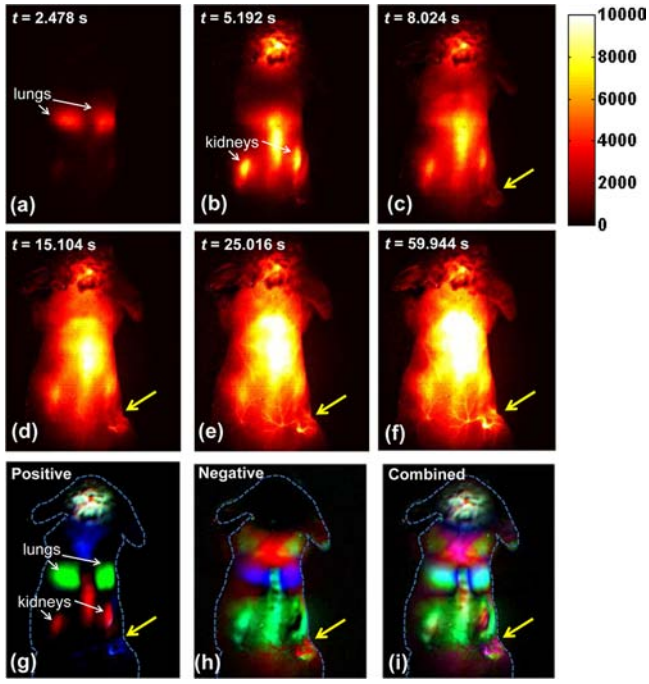

Figure 2. Time course NIR-II fluorescence images and dynamic contrast-enhanced images based on PCA analysis: (a−f) NIR-II fluorescence images of a 4T1 tumor bearing mouse after injection of a 200 μL solution containing 0.35 mg/mL SWNTs; (g) positive pixels from PCA, showing lungs, kidneys, and major vessels in the tumor; (h) negative pixels from PCA, showing the body of the tumor; (i) overlaid image showing the absolute value of both positive and negative pixels, from which both the vessels in the tumor and the tumor outline can be seen. Yellow arrows in the images highlight the tumor.

To gain further anatomical information of the tumor, PCA was applied to a time series of the first 200 fluorescence images (within 23.8 s pi). Previous work showed PCA as a powerful

dx.doi.org/10.1021/ja303737a | J. Am. Chem. Soc. 2012, 134, 10664−10669

tool of discriminating organs based on their different blood circulating behaviors, since PCA turns pixels into groups (components) based on their variance, i.e., PCA groups pixels that vary similarly in time.[11,29] The pixel intensity in the tumor region differed from other organs as blood flowed later into the tumor than normal organs such as lungs, liver, and kidneys, presumably because of the small size and random structure of newly born vessels. This difference, unique to tumors, allowed us to pick up the tumor as a single component from PCA, as shown in Figure 2g–i. The positive pixel image in Figure 2g showed major vessels in the tumor color-coded in cyan, along with lungs and kidneys that could also be identified easily. The negative pixel image in Figure 2h showed the main body of the tumor, color-coded in chartreuse, which made the tumor a distinct component from all other organs. Moreover, the combined image in Figure 2i overlaid both positive and negative images and allowed us to visualize both the tumor outline (chartreuse) and vasculature inside the tumor (magenta). Interestingly, it was not until ~60 s pi (Figure 2f) that the tumor outline became distinguishable from nearby skin in the video, while all others organs were even brighter than the tumor. However, PCA analysis based on only the first frames within 23.8 s pi was able to delineate the tumor distinctly from all other normal tissues and organs, suggesting PCA as a useful tool for immediate tumor detection. We reproduced this finding on three other mice.

By collecting blood at various time points after injection and measuring the blood SWNT concentration using Raman spectroscopy,[26] we were able to extrapolate the blood circulation half-life of approximately 30 h (Figure 3a). Because of the extremely long circulation of SWNTs and continuous accumulation of SWNTs in the tumor interstitial space owing to the enhanced permeability and retention (EPR) effect,[32] a steady increase of NIR fluorescence in the tumor region was observed on all injected mice, as shown in the time course NIR images taken on one of the mice (n = 4) over a 72 h time period (Figure 4a–d). To quantify the biodistribution of the

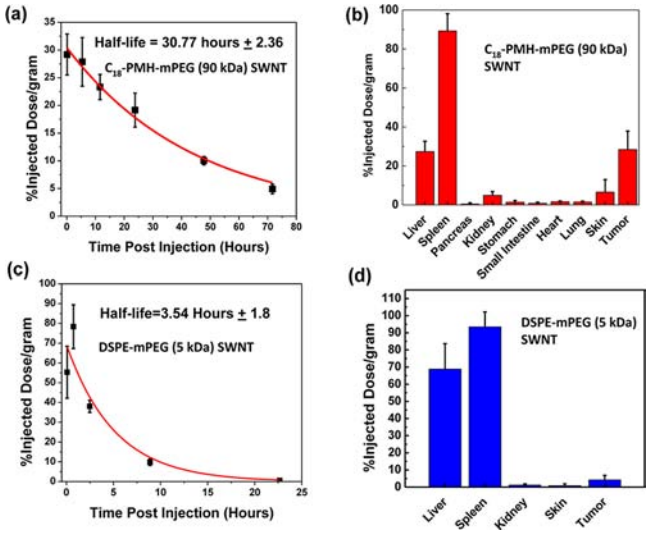

Figure 3. (a) Concentration of SWNTs (black symbols) in blood vs time measured for an injected 90 kDa C_{18}-PMH-mPEG SWNT solution (see Experimental Details). A first-order exponential decay model was used for fitting (red curve). (b) Biodistribution of the 90 kDa C_{18}-PMH-mPEG SWNTs in various organs measured by collecting organs from the mice (n = 4) 100 h after injection (see Experimental Details). (c) Circulation and (d) biodistribution of DSPE-mPEG (5 kDa) coated SWNT in vivo (n = 3).

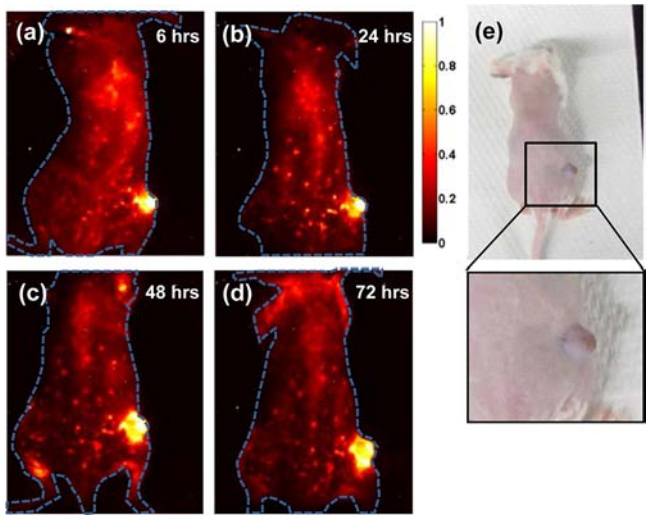

Figure 4. NIR-II imaging of xenograft 4T1 tumor with high uptake of SWNTs. (a–d) Time course NIR-II fluorescence images of the same mouse injected with C_{18}-PMH-mPEG (90 kDa) coated SWNTs, showing increasing tumor contrast due to the accumulation of nanotubes inside the tumor. (e) Digital camera image of the same mouse as shown in (a–d), with noticeable darkening of the tumor due to the high tumor uptake of SWNTs.

SWNTs, mouse organs (n = 4) were collected 100 h after SWNT injection (see Experimental Details).[26] There was no toxicity observed in the mice after the injection of SWNTs. Previous studies have investigated the long-term biodistribution, blood chemistry, and toxicity of SWNTs coated with phospholipid-PEG[33] and DSPE-mPEG/larger 1 MDa C_{18}-PMH-mPEG.[17] In both studies, there was no indication of long-term toxicity. The clearance of the phospholipid-PEG SWNTs occurred primarily through the biliary pathway (feces) with a small portion of the SWNTs being excreted through renal filtration (urine).[33] The 30% injected dose (ID) per gram of tumor uptake (Figure 3b) is one of the highest known tumor accumulations of intravenously injected nanoparticles ever observed, according to our survey of the literature. The tumor visibly darkened 72 h after SWNT injection (Figure 4e), highlighting the significant accumulation in cancerous tissue. Previously, the highest reported tumor uptake of SWNTs was 23% ID/g,[22] which had high skin uptake of SWNTs, making it undesirable for imaging. Note that attaching targeting ligands to SWNTs could lead to further improvement of tumor uptake.[34]

The reduction in size of the C_{18}-PMH-mPEG surfactant could be a contributing factor in the 80% reduction in skin accumulation of the SWNTs. It has been speculated that the larger, 1 MDa C_{18}-PMH-mPEG coated SWNTs became trapped in the dermis because of their bulky size;[22] 90 kDa C_{18}-PMH-mPEG SWNTs may avoid entrapment in the skin because of the smaller hydrodynamic radius. However, we do not have definitive proof of why the smaller C_{18}-PMH-mPEG SWNTs have lower skin uptake, and this is an ongoing area of investigation.

We further examined the blood circulation behavior and tumor accumulation of SWNTs functionalized by several popular types of surfactants, including 1,2-distearoylphosphatidylethanolaminemethylpoly(ethylene gly-

dx.doi.org/10.1021/ja303737a | J. Am. Chem. Soc. 2012, 134, 10664–10669

col) (DSPE-mPEG, 5 kDa) (Figure 3c). DSPE-mPEG coated SWNTs had a circulation half-life of ~3.5 h and tumor accumulation of 4% ID/g. These data support the assertion that a long circulation time is necessary for high tumor uptake of nanoparticles. A particle with more passes through the fenestrated tumor vasculature increases the overall probability of tumor uptake.[35,36]

To reveal the spatial distribution of SWNTs accumulation, a tumor was collected and fixed for microtome slicing 100 h after SWNT injection. The tumor, with volume of ~20 mm^3, yielded 45 slices each with ~40 μm thickness. Using rat anti-mouse CD31 and Cy5 labeled anti-rat IgG antibodies, we stained all tumor slices and imaged the location of the CD31 proteins, using the Cy5 emission at ~700 nm upon excitation at 658 nm. CD31 is commonly found at sites of angiogenesis,[37] and therefore, anti-mouse CD31 has been widely used as an indicator of blood vessels. In our case rat anti-mouse CD31 bound to mouse CD31 in the blood vessels and a secondary antibody, Cy5 labeled anti-rat IgG, bound to rat anti-mouse CD31 in order to visualize the distribution of CD31 for fluorescence imaging.

For every slice we imaged the blood vessels stained by Cy5 and SWNT NIR-II fluorescence excited by the same 658 nm excitation. A 10× objective was used to block-scan the whole slice (5 mm × 6 mm) with a step size of 200−500 μm. We then overlaid the blood vessels (color-coded in green) and SWNTs (color-coded in red) to assess colocalization (Figure 5a). The

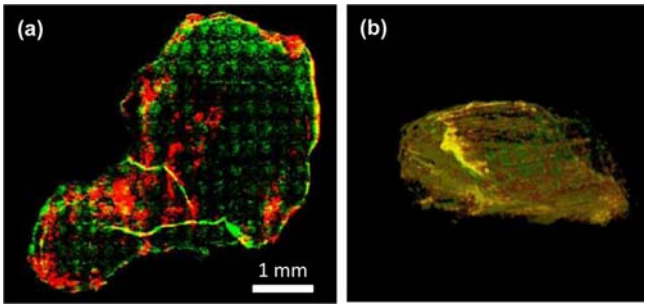

Figure 5. Ex vivo imaging of 4T1 murine tumor slices with high SWNT uptake. (a) Tumor slice from a tumor showing the location of SWNTs (coded in red) and Cy5-labeled anti-mouse CD31 (coded in green) and their colocalization (yellow). (b) Reconstructed 3D snapshot image taken from the second Supporting Information video file with the same color coding as in (a).

overlaid image of a tumor slice revealed most of the SWNTs (in red and yellow regions) located at the peripheral area of the tumor. We did observe vascular structures deep inside the tumor color-coded in yellow due to SWNT colocalization with large vessel structures inside the tumor (Figure 5a). We imaged all of the tumor slices of an entire tumor and then reconstructed the tumor in 3D using the ImageJ software (see second and third Supporting Information video files and a snapshot in Figure 5b). Overall, a high degree of colocalization of SWNT and major vessels in the tumor was observed (abundant yellow colors, Figure 5b) while the small vascular structures appeared impermeable to the SWNTs (green colors in Figure 5).

CONCLUSIONS

Achieving high tumor uptake of C_{18}-PMH-mPEG (90 kDa) coated SWNTs after intravenous injection allowed for improved detection by NIR-II imaging. The accumulation of SWNTs inside the tumor steadily increased over 72 h pi, owing to the extremely long circulation of nanotubes. The high tumor uptake could potentially be used to push the lower size limit of tumor detection and imaging. Colocalization analysis based on tumor slice imaging and 3D reconstruction revealed distribution of SWNTs mainly in the highly vascularized region and the edges of the tumor. Substantial extravasation of SWNTs was also observed. The combined high tumor accumulation ability and ideal fluorescence excitation/emission properties make SWNTs excellent candidates for nanomedicine.

EXPERIMENTAL DETAILS

Synthesis of C_{18}-PMH-mPEG Polymer. Octadecene (0.606 g, 2.4 mmol) and maleic anhydride (0.235 g, 2.4 mmol, freshly recrystallized from toluene) were added to a 10 mL flask, followed by the addition of 4 mL of anhydrous dioxane. After all the solids were dissolved, azobisisobutyronitrile (AIBN, 0.100 g, 0.60 mmol, freshly recrystallized from methanol) was added. The flask was installed with a condenser and closed with a rubber stopper. The reaction system was vacuumed to remove air and then back-filled with nitrogen. Such a sequence was repeated 3 times. The reaction system was heated to 100 °C under nitrogen protection for 6 h. After the mixture cooled to room temperature, the solution was added dropwise to 50 mL of cold methanol. The polymer was collected by centrifugation and reprecipitated from tetrahydrofuran (THF) into cold methanol. The polymer was collected by centrifuge and dried under vacuum for 1 day. The product was collected as a white solid (yield 70%, M_n = 3.2 kDa, PDI = 1.1). Molecular weights and distributions of polymers were determined by using a Waters GPC liquid chromatograph equipped with a Waters 515 HPLC pump, a Waters 2414 refractive index detector, and a Waters 2489 UV−visible detector. Polystyrene standards (Aldrich) were used for calibration, and THF was used as the eluent.

An amount of 10 mg of the poly(maleic anhydride-alt-1-octadecene) product was added to 13.5 mL of dimethyl sulfoxide and 1.5 mL of pyridine. An amount of 285.7 mg of methoxy-terminated poly(ethylene glycol) amine (5 kDa MW) was then added to the solution, which was stirred at room temperature for 12 h. Next, 22.7 mg of 1-ethyl-3-(3-dimethylaminopropyl)carbodiimide (EDC) was added to the solution which continued to stir at room temperature for 24 h. The solution was dialyzed against water through dialyzing membrane (12−14 kDa MWCO) with 8× water changes to remove any unreacted methoxy-terminated poly(ethylene glycol) amine or poly(maleic anhydride-alt-1-octadecene). The resulting C_{18}-PMH-mPEG product was then lyophilized and stored at −20 °C until use.

In order to determine the degree of PEGylation of the C_{18}-PMH-mPEG, we performed ^{1}H NMR in $CDCl_3$ (300 MHz). The peaks from 3.3 to 3.8 ppm (broad, CH_2 from mPEG) and 1.1−1.3 (CH_2 from the C_{18} chain) were compared. The ratio was about (25−26):1, indicating that the C_{18}-PMH precursor was fully PEGylated. ^{1}H NMR (300 MHz, $CDCl_3$) δ: 3.3−3.8 (m, br, CH_2 of mPEG), 1.1−1.3 (m, CH_2 of C_{18} chain), 0.88 (m, br, CH_3 of C_{18}-PMH). In order to confirm that the C_{18}-PMH-mPEG does not degrade during bath sonication, the surfactant was sonicated at a 1 mg/mL for 1 h, followed by 4× dialysis against water with a 12−14 kDa MWCO dialysizing membrane to remove any detached or degraded PEG chains. ^{1}H NMR in $CDCl_3$ (300 MHz) of the sonicated C_{18}-PMH-mPEG showed a similar spectrum, with the peaks at 3.3−3.8 ppm (broad, CH_2 from mPEG) and 1.1−1.3 (CH_2 from the C_{18} chain) having a 24:1 ratio, indicating that the C_{18}-PMH-mPEG remains intact after sonication.

Preparation of Biocompatible SWNTs. 0.2 mg/mL HiPCO SWNTs (Unidym) and 1 mg/mL 90 kDa C_{18}-PMH-mPEG were added to 10 mL of deionized ultrafiltered (DIUF) water and bath-sonicated for 1 h. Following sonication, 2.5 mL of 10× phosphate buffered saline (PBS) was added to the solution. The SWNT suspension was then centrifuged at 22000g for 6 h to remove any aggregates and uncoated nanotubes. The supernatant was then

dx.doi.org/10.1021/ja303737a | J. Am. Chem. Soc. 2012, 134, 10664−10669

collected and analyzed by atomic force microscopy to ensure that only individual SWNTs remained (data not shown). The SWNT solution was then washed 8 times by centrifuge filtration in DIUF water with a 100 kDa MWCO (Millipore) to remove any excess polymer though some excess polymer remained in solution after washing. The final SWNT solution was concentrated down in 2× phosphate buffer saline (PBS) using the 100 kDa MWCO centrifuge filter and centrifugation at 4000*g* for 15 min. The concentrated SWNT remains above the membrane filter. Then 2× phosphate buffer saline is used to mimic the pH and salt concentration found in the blood; any intravenous injection needs to be in 2× PBS in order not to harm the mouse by rapidly shifting the buffer and pH of the blood. The SWNT concentration was brought to 0.35 mg/mL as determined by UV−vis−NIR spectroscopy (Cary 6000i) based on a mass extinction coefficient of SWNTs of 46.5 L/(g·cm) at 808 nm.[17]

To determine the degree of surfactant functionalization of the SWNTs, we lyophilized 1 mL of 0.5 mg/mL SWNT solution and weighed the resulting solid. The weight was 4.33 mg, indicating that there was approximately a 7.66:1 weight ratio of 90 kDa C_{18}-PMH-mPEG surfactant/SWNT. This was equivalent to 9.67 C_{18}-PMH-mPEG molecules/100 nm of SWNT.

For DSPE-mPEG SWNT, 0.2 mg/mL HiPCO SWNTs (Unidym) and 1 mg/mL 1,2-distearoylphosphatidylethanolaminemethylpoly-(ethylene glycol) (DSPE-mPEG, 5 kDa, Laysan Bio Inc.) were added to 10 mL of deionized ultrafiltered (DIUF) water and bath-sonicated for 1 h. SWNTs were then centrifuged and washed in the same manner as the C_{18}-PMH-mPEG SWNT.

For 1−2 MDa C_{18}-PMH-mPEG SWNT, 0.2 mg/mL HiPCO SWNTs (Unidym) and 1 mg/mL 1 MDa C_{18}-PMH-mPEG were added to 10 mL of deionized ultrafiltered (DIUF) water and bath-sonicated for 1 h. SWNTs were then centrifuged and washed in the same manner as the 90 kDa C_{18}-PMH-mPEG coated SWNTs.

Dynamic light scattering (DLS) was used to determine the hydrodynamic radius of the SWNT solutions using a Brookhaven Instruments 90Plus particle size analyzer and a 1 cm quartz cuvette. A 0.05 mg/mL concentration of SWNT in water was used for all DLS measurements.

Atomic force microscopy (AFM) was used to show the size of 90 kDa C_{18}-PMH-mPEG coated SWNTs as well as demonstrate the coating on the SWNTs. To prepare the SWNTs for AFM, 50 μL of a 0.05 mg/mL SWNT solution was placed on 1 cm silicon substrate for 20 min that was presoaked in 3-aminopropyltriethoxysilane (APTES) .

Mouse Injection and Handling. BALB/c mice (n = 4) were purchased from Charles River and were housed at Stanford Research Animal Facility under Stanford Institutional Animal Care and Use Committee protocols. When they reached 8 weeks in age, mice were inoculated with 1 million 4T1 cells (ATCC No. CRL-2539) on the right hind limb. Tumors were allowed to grow for 7 days, at which point they were ∼20−50 mm^3 in volume. The tumor size was monitored with digital calipers. On day 7, 200 μL of 0.35 mg/mL SWNT solution in 2× PBS buffer was injected intravenously through the tail, and video-rate imaging was taken during and after injection. The mice did not experience any weight loss or change in behavior after injection. To anesthetize the mice for injection and subsequent imaging, the mice were placed in a knockdown box that had 2 L/min O_2 with 2.5% isoflurane flowing through it.

Video-Rate NIR Imaging. Video-rate NIR imaging was carried out on a home-built setup consisting of a 2D InGaAs camera (Princeton Instruments). The geometry of the imaging setup can be found in our previous publication.[11] The excitation light was provided by a fiber-coupled 808 nm diode laser (RMPC Lasers), chosen to overlap with the traditional biological transparency window and thus to afford maximum penetration. The light was collimated by a 4.5 mm focal length collimator (ThorLabs) and filtered by an 850 nm short pass filter (ThorLabs FES850) to remove unwanted radiation in the emission range. The excitation spot was a circle with a diameter of approximately 6 cm. The output excitation power was ∼6 W, leading to power density of approximately 0.2 W/cm^2. Emitted light was passed through a 1100 nm long-pass filter (ThorLabs FEL1100) and focused onto the detector by a lens pair consisting of two NIR achromats (200 and 75 mm, Thorlabs). The camera was set to expose continuously with an exposure time of 100 ms, and images were acquired with a frame rate of 8.4 frame/s because of a 19 ms overhead in the readout. Then 1800 consecutive frames were collected, leading to a total imaging time of 214.2 s. Four BALB/c mice were used, and results shown are representative.

Postinjection NIR Imaging. Mice (n = 4) injected with 200 μL of 0.35 mg/mL C_{18}-PMH-mPEG (90 kDa) coated SWNT suspension were imaged at 6, 24, 48, and 72 h postinjection. The same 808 nm laser excitation cleaned by an 850 nm short-pass filter and 2D InGaAs camera equipped with 1100 nm long-pass filter were used as in the video-rate imaging. An exposure time of 300 ms was used to take still images of fluorescence in the 1.1−1.4 μm NIR region. Representative NIR fluorescence images on the same mouse were shown after flat field correction for any nonuniformity of excitation beam.

Ex Vivo Biodistribution and Circulation. An amount of 4−8 μL of blood was collected from the tail artery of the mice (n = 4) at various time points after injection of 200 μL of 0.35 mg/mL C_{18}-PMH-mPEG (90 kDa) coated SWNTs. Then 8 μL of tissue lysis buffer was added to each blood sample. The samples were bath-sonicated for 30 s to create a homogeneous solution. By use of a 785 nm laser diode as the excitation source, the Raman scattering spectrum from the solution was collected. The area under the SWNT graphitic "G" peak was integrated after background subtraction. This was done 3 times for each sample to get an average value from which the percent injected dose per gram of tissue could be calculated after normalization to the "G" peak area for the injected solution.

At 100 h after injection of SWNT solution, the mice (n = 4) were sacrificed and organs were collected in individual vials and weighed. A 2% sodium cholate solution in 1 mL of Solvable was added to each vial, followed by heating at 70 °C for 2 h to dissolve the organs and create a homogeneous solution. The same protocol for circulation was used for collecting the Raman and determining the % ID/g of the organs.

For characterization of DSPE-mPEG SWNT biodistribution and circulation, the same protocol as above was used on three mice.

Tumor Slice Staining. For one of the tumor bearing mice, after 200 μL of 0.35 mg/mL C_{18}-PMH-mPEG (90 kDa) coated SWNT solution was intravenously injected, the mouse was sacrificed 100 h after injection and the tumor was dissected and immediately placed in optimal cutting temperature (OCT) compound, frozen with liquid nitrogen, and stored at −80 °C. By use of a Heidelberg microtome, 40 μm thick slices of the tumor were collected and placed on Superfrost Plus glass substrates, 45 slices in total, leading a total thickness of 1.8 mm for the tumor. The tumor slices were soaked in cold acetone for 10 min, washed three times with 1× PBS, and then incubated in protein block (3% FBS in 1× PBS Tween) overnight at 4 °C. Following a wash by 1× PBS-Tween (0.05%), 0.039 μg/mL (300 pM) rat anti-mouse CD31 (BD Pharmingen) was incubated with the slices in a 10% FBS/80% 1× PBS/10% 1× PBS-Tween (0.05%) solution for 3 h. The tumor slices were then washed twice with 1× PBS-Tween (0.05%) and incubated with Cy5-labeled anti-rat IgG (H + L) antibody (Jackson Immuno Research).

Tumor Slice Imaging and 3D Reconstruction. To determine the location of SWNTs in each tumor slice, a 658 nm laser diode cleaned by 750 nm short-pass filter (Thorlabs) with an 800 μm diameter spot was focused by a 10× objective lens (Bausch and Lomb). The resulting CNT fluorescence was collected using a 2D InGaAs camera (Princeton Instruments) equipped with an 1100 nm long-pass filter (Thorlabs) at an exposure time of 300 ms. Because of the larger size of each tumor slice compared with the field of view, the 10× objective block-scanned the whole slice with a step size of 426 μm in x and 518 μm in y, leading to each block of 426 μm × 518 μm. LabVIEW was used to control the block-scanning and to stitch all images to form a large image. To image Cy5-labeled anti-mouse CD31 in each tumor slice, the same 658 nm laser diode cleaned by a 655 nm (40 nm bandwidth) band-pass filter (Semrock) with an 800 μm diameter spot was focused by a 10× objective lens (Bausch and Lomb). The resulting CNT fluorescence was collected using a Si CCD camera (Hamamatsu) equipped with a 716 nm (40 nm bandwidth)

band-pass filter (Semrock) at an exposure time of 100 ms. Because of the larger size of each tumor slice compared with the field of view, the 10× objective block-scanned the whole slice with a step size of 280 μm in x and 360 μm in y, leading to each block of 280 μm × 360 μm. LabVIEW was used to control the block-scanning and to stitch all images to form a large image. Matlab 7 was used to color-code SWNT fluorescence in red and Cy5 in green and to overlay the two channels. ImageJ was then used to reconstruct the 3D image based on all 45 slice images.

SWNT in Vitro Toxicity Assay. A MTS colorimetic assay kit, CellTiter96 (Promega), was used to determine the 90 kDa C_{18}-PMH-mPEG SWNT cytotoxicity in vitro. 4T1 murine breast cancer cells (ATCC No. CRL-2539) were added to a 96 well plate (7500 cells/well) and incubated with 100 μL of 1640 RPMI medium and serially diluted SWNTs (n = 4). Cells were incubated for 24 h at 5% CO_2 and 37 °C. Afterward, the SWNTs and old medium were replaced with fresh medium and 15 μL of CellTiter96. Initial absorbance readings were taken for each well. After 1 additional hour of incubation, absorbance readings were taken again and the absorbance change was correlated to cell viability.

■ ASSOCIATED CONTENT

Ⓢ Supporting Information

Further characterization of the SWNTs and three videos of the SWNTs in the mouse after injection and 3D reconstruction of a SWNT containing tumor. This material is available free of charge via the Internet at http://pubs.acs.org.

■ AUTHOR INFORMATION

Corresponding Author

hdai@stanford.edu

Author Contributions

†These authors contributed equally.

Notes

The authors declare no competing financial interest.

■ ACKNOWLEDGMENTS

This work was supported by the National Institutes of Health (NIH-NCI) (Grant 5R01A135109-02).

■ REFERENCES

(1) Wagner, V.; Dullaart, A.; Bock, A. K.; Zweck, A. *Nat. Biotechnol.* **2006**, *24*, 1211−1217.
(2) Jain, R. K.; Stylianopoulos, T. *Nat. Rev. Clin. Oncol.* **2010**, *7*, 653−664.
(3) Stroh, M.; Zimmer, J. P.; Duda, D. G.; Levchenko, T. S.; Cohen, K. S.; Brown, E. B.; Scadden, D. T.; Torchilin, V. P.; Bawendi, M. G.; Fukumura, D.; Jain, R. K. *Nat. Med.* **2005**, *11*, 678−682.
(4) Allen, P. M.; Liu, W.; Chauhan, V. P.; Lee, J.; Ting, A. Y.; Fukumura, D.; Jain, R. K.; Bawendi, M. G. *J. Am. Chem. Soc.* **2009**, *132*, 470−471.
(5) Duncan, R. *Nat. Rev. Cancer* **2006**, *6*, 688−701.
(6) Lim, Y. T.; Kim, S.; Nakayama, A.; Stott, N. E.; Bawendi, M. G.; Frangioni, J. V. *Mol. Imaging* **2003**, *2*, 50−64.
(7) Terentyuk, G. S.; Maslyakova, G. N.; Suleymanova, L. V.; Khlebtsov, N. G.; Khlebtsov, B. N.; Akchurin, G. G.; Maksimova, I. L.; Tuchin, V. V. *J. Biomed. Opt.* **2009**, *14*, 021016.
(8) Smith, A. M.; Mancini, M. C.; Nie, S. *Nat. Nanotechnol.* **2009**, *4*, 710−711.
(9) Welsher, K.; Liu, Z.; Sherlock, S. P.; Robinson, J. T.; Chen, Z.; Daranciang, D.; Dai, H. *Nat. Nanotechnol.* **2009**, *4*, 773−780.
(10) Frangioni, J. V. *Curr. Opin. Chem. Biol.* **2003**, *7*, 626−634.
(11) Welsher, K.; Sherlock, S. P.; Dai, H. *Proc. Natl. Acad. Sci. U. S. A.* **2011**, *108*, 8943−8948.
(12) Lakowicz, J. R. *Subcell. Biochem.* **1988**, *13*, 89−126.
(13) Gordon, R.; Herman, G. T. *Int. Rev. Cytol.* **1974**, *38*, 111−151.
(14) Maeda, H.; Wu, J.; Sawa, T.; Matsumura, Y.; Hori, K. *J. Controlled Release* **2000**, *65*, 271−284.
(15) Liu, Z.; Chen, K.; Davis, C.; Sherlock, S. P.; Cao, Q.; Chen, X.; Dai, H. *Cancer Res.* **2008**, *68*, 6652−6660.
(16) Prencipe, G.; Tabakman, S. M.; Welsher, K.; Liu, Z.; Goodwin, A. P.; Zhang, L.; Henry, J.; Dai, H. *J. Am. Chem. Soc.* **2009**, *131*, 4783−4787.
(17) Robinson, J. T.; Welsher, K.; Tabakman, S. M.; Sherlock, S. P.; Wang, H. L.; Luong, R.; Dai, H. *Nano Res.* **2010**, *3*, 779−793.
(18) Liu, Z.; Robinson, J. T.; Tabakman, S. M.; Yang, K.; Dai, H. *Mater. Today* **2011**, *14*, 316−323.
(19) De La Zerda, A.; Zavaleta, C.; Keren, S.; Vaithilingam, S.; Bodapati, S.; Liu, Z.; Levi, J.; Smith, B. R.; Ma, T. J.; Oralkan, O.; Cheng, Z.; Chen, X.; Dai, H.; Khuri-Yakub, B. T.; Gambhir, S. S. *Nat. Nanotechnol.* **2008**, *3*, 557−562.
(20) De La Zerda, A.; Liu, Z.; Bodapati, S.; Teed, R.; Vaithilingam, S.; Khuri-Yakub, B. T.; Chen, X.; Dai, H.; Gambhir, S. S. *Nano Lett.* **2010**, *10*, 2168−2172.
(21) Welsher, K.; Liu, Z.; Daranciang, D.; Dai, H. *Nano Lett.* **2008**, *8*, 586−590.
(22) Liu, X.; Tao, H.; Yang, K.; Zhang, S.; Lee, S. T.; Liu, Z. *Biomaterials* **2010**, *32*, 144−151.
(23) Matsumura, Y.; Maeda, H. *Cancer Res.* **1986**, *46*, 6387−6392.
(24) Iyer, A. K.; Khaled, G.; Fang, J.; Maeda, H. *Drug Discovery Today* **2006**, *11*, 812−818.
(25) Robinson, J. T.; Tabakman, S. M.; Liang, Y.; Wang, H. L.; Sanchez Casalongue, H.; Vinh, D.; Dai, H. *J. Am. Chem. Soc.* **2011**, *133*, 6825−6831.
(26) Liu, Z.; Tabakman, S. M.; Welsher, K.; Dai, H. *Nano Res.* **2009**, *2*, 85−120.
(27) Tagmatarchis, N.; Prato, M. *J. Mater. Chem.* **2004**, *14*, 437−439.
(28) Prato, M.; Kostarelos, K.; Bianco, A. *Acc. Chem. Res.* **2008**, *41*, 60−68.
(29) Hillman, E. M. C.; Moore, A. *Nat. Photonics* **2007**, *1*, 526−530.
(30) Folkman, J. *Semin. Cancer Biol.* **1992**, *3*, 65−71.
(31) Shirinifard, A.; Gens, J. S.; Zaitlen, B. L.; Popławski, N. J.; Swat, M.; Glazier, J. A. *PLoS One* **2009**, *4*, e7190.
(32) Gao, X. H.; Cui, Y. Y.; Levenson, R. M.; Chung, L. W. K.; Nie, S. *Nat. Biotechnol.* **2004**, *22*, 969−976.
(33) Liu, Z.; Davis, C.; Cai, W.; He, L.; Chen, X.; Dai, H. *Proc. Natl. Acad. Sci. U.S.A.* **2008**, *105*, 1410−1415.
(34) Liu, Z.; Cai, W.; He, L.; Nakayama, N.; Chen, K.; Sun, X.; Chen, X.; Dai, H. *Nat. Nanotechnol.* **2007**, *2*, 47−52.
(35) Bagalkot, V.; Kyung Yu, M.; Jon, S. Nanoparticles for Combined Cancer Imaging and Therapy. In *Nanoplatform-Based Molecular Imaging*; Chen, X., Ed.; John Wiley & Sons, Inc.: Hoboken, NJ, 2011; pp 565−592.
(36) Wong, C.; Stylianopoulos, T.; Cui, J.; Martin, J.; Chauhan, V. P.; Jiang, W.; Popović, Z.; Jain, R. K.; Bawendi, M. G.; Fukumura, D. *Proc. Natl. Acad. Sci. U.S.A.* **2011**, *108*, 2426−2431.
(37) Giatromanolaki, A.; Koukourakis, M. I.; Theodossiou, D.; Barbatis, K.; O'Byrne, K.; Harris, A. L.; Gatter, K. C. *Clin. Cancer Res.* **1997**, *3*, 2485−2492.